CHAPTER 6

CONCLUSION

The frame of this work was the evolution of microelectronic SOI technologies for microwave applications. Performances, potentialities of various kinds of passive elements and MOSFET transistors fabricated on classical, high resistivity SOI, and Silicon-on-Sapphire technologies were studied. All these components are keystones to develop RF circuits like low noise amplifiers (LNA), or oscillators.

Since the technology is evolving quickly, all methods used to measure and characterize integrated components have to be checked. Also the structure used to measure components must be re-designed to follow the technological evolutions.

The characterization of integrated devices requires accurate on-wafer measurement techniques. As described in Chapter 2, on-wafer measurements are a hot topic, which requires several critical steps. The method used during this work is mainly the two-step calibration. A first calibration (TRM) is made using a commercial calibration substrate, and another (TRL) is made on-wafer, by measuring standards fabricated close to the device of interest. This last calibration suffers from some limitations. The main problem is the determination of the characteristic impedance of the line used during the calibration. Two well-known methods have been explained, and a new one, based on the measurement of two lines, has been developed and validated up to 40GHz. Contrary to other methods, the new method does not require more standards than the TRL. Less measurements are needed, and less area is used on the wafer for the on-wafer calibration.

For several years now, SOI CMOS exhibits its benefit in the fields of low cost, efficient RF circuits. In order to use properly and efficiently integrated MOSFET transistors, they must be accurately characterized on a wide frequency band. A systematic procedure, successfully applied to various SOI transistors has been proposed in Chapter 3 to determine the most relevant equivalent circuit of SOI MOSFET.

When the equivalent circuit is defined, the values of each of its components must be determined. These elements are usually divided into two groups, the intrinsic components, which are function of the active part of the transistor, and the extrinsic, which are function of the geometry of the transistor. An accurate determination of the values of the extrinsic parameters is necessary to obtain physical values for the intrinsic ones. If the extrinsic components are not accurately determined, or if the used equivalent circuit does not correspond to the physics of the device, the intrinsic components, which are supposed to be constant versus frequency, will be frequency dependent.

Within this field, a new method has been proposed to determine accurately parasitic capacitances. This method allows us to extract from measurements parasitic capacitances, called “extrinsic-extrinsic”, that were estimated previously by using electrostatic simulation.

The proposed extraction procedure has been applied successfully to FD and PD deep sub-micron SOI MOSFETs ($L = 0.13\mu m$).

By reducing the gate length of the transistors, the analog performances of MOSFET for RF applications are usually improved. But this requires an increase of the fabrication process complexity.

Other techniques can be used to increase the performance of a SOI CMOS technology without any drastic reduction of the gate length. In Chapter 4, two alternative structures of MOSFET, the Dynamic Threshold MOSFET and the Graded Channel MOSFET, have been studied into details, from DC to RF. The DTMOS allows us to reduce the threshold voltage of MOSFET and to reach the maximal performances under a lower applied voltage than for a conventional MOSFET. Furthermore, when the transistors are used at low frequencies, below 200 MHz in our experiment, the DTMOS benefits of the dynamic modulation of its body, which results into a significant increase of its transconductance and of its intrinsic gain. Unfortunately, the performances of DTMOS are mainly limited by the value of the gate to body resistance, which will drastically increase in the next generation of PD transistors. Indeed, this resistance is nearly inversely proportional to the floating body thickness. And it reduces each time the technology evolves.

The GCMOS allows us to increase significantly the gain compared to MOSFET with the same gate length, and especially when the gate voltage overdrive is low. Also, the asymmetrical doping profile of the channel provides to the GCMOS an extremely low output conductance due to its double saturation regime. Fully CMOS compatible, this transistor structure is probably the most promising alternative structure studied. Indeed, in a few years, the future structure of MOSFET transistors will probably be Double Gate structure. In such configuration, the active film of silicon is fully depleted, thus there is no floating body under the transistor channel. DTMOS or other body-contacted devices will not have any interest at that time, as they will not be able to control the body potential efficiently. But asymmetric doped transistors, like GCMOS, will still be interesting if the channel doping process is still controlled precisely for transistors with a gate length close to a few tens of nanometer.

In parallel with the analysis of conventional and alternative transistor, integrated passive components have been studied too. By using the latest evolution in microelectronics, various topologies of transmission lines, like CPW or TFMS, have been analyzed. From this original study, we consider that TFMS transmission line is the most interesting transmission line topology for future high frequency circuit, as it is not influenced by the substrate. A 50 Ω TFMS line, fabricated during this work on a technology with 6 metal levels using medium or high resistivity silicon substrate, exhibits twice the losses of CPW lines made on a high resistivity substrate (TFMS: .8dB/mm@20GHz ><CPW: .4dB/mm@20GHz). But simulations have demonstrated that in next generations of CMOS process, when 8 metal level will be available, 50 Ω TFMS lines should exhibit nearly the same attenuation coefficient as CPW lines made on HRS substrate.

Also, a new physical model of integrated inductors has been developed. This model, based on a coupled line analysis of square spiral inductors, is scalable and independent of the technology used. Inductors with various spacings between strips, conductor widths, or number of turns can be simulated on different multi-layered substrates. Each layer that composes the substrate is defined using its electrical properties (permittivity, permeability, conductivity). Thus a correct estimation of the substrate losses is obtained.

This model is more than just a CAD tool. It allows us to predict the influence of the substrate and to optimize the geometry of inductances in new technologies. By using this tool and experimental results, general guidelines are provided to help the design of integrated inductors.

The influence of magnetic material, ground plane…, on the performance of integrated inductors can also be studied with this model before any fabrication process, by using relatively few computer power.

In the present work, elementary SOI integrated components have been studied into details. Properties and performances of active and passive components have been analyzed in order to allow the design of efficient RF analog circuit. The study of alternative MOSFETs has demonstrated the benefit of the DTMOS and GCMOS compared to conventional MOSFETs for low power RF applications. Some study should still be performed on these devices, such as large-signal modeling and noise characterization.

The emergence of commercial CMOS processes using several metal layers has given the opportunity to study new kinds of integrated transmission lines. The interest of TFMS lines for future generations of MMIC has been demonstrates. More than just providing low loss interconnections, TFMS could bring more flexibility in the design of passive elements for high frequency applications. It is then possible to optimize passive elements in the same way it is done in the design of microwave hybrid circuits, and also to optimize the size of active devices as it is done in microelectronics.

APPENDIX A

RELATIONS BETWEEN SCATTERING AND IMMITTANCE PARAMETERS

Practically, the measured devices are usually 2-ports, referenced to the same generator impedance at both accesses. In that case, some general relations provided in Chapter 2 can be simplified, providing practical and useful relations. In the following tables, the *pseudo scattering* and immitance parameters are expressed as a function of each others. Considering that the generator impedances at both ports is equal to Z_0.

	S	Y	Z
S	$s_{11} = s_{11}$	$s_{11} = \frac{(1-y'_{11})(1+y'_{22})+y'_{12}y'_{21}}{(1+y'_{11})(1+y'_{22})-y'_{12}y'_{21}}$	$s_{11} = \frac{(z'_{11}-1)(z'_{22}+1)-z'_{12}z'_{21}}{(1+z'_{11})(1+z'_{22})-z'_{12}z'_{21}}$
	$s_{12} = s_{12}$	$s_{12} = \frac{-2y'_{12}}{(1+y'_{11})(1+y'_{22})-y'_{12}y'_{21}}$	$s_{12} = \frac{2z'_{12}}{(1+z'_{11})(1+z'_{22})-z'_{12}z'_{21}}$
	$s_{21} = s_{21}$	$s_{21} = \frac{-2y'_{21}}{(1+y'_{11})(1+y'_{22})-y'_{12}y'_{21}}$	$s_{21} = \frac{2z'_{21}}{(1+z'_{11})(1+z'_{22})-z'_{12}z'_{21}}$
	$s_{22} = s_{22}$	$s_{22} = \frac{(1+y'_{11})(1-y'_{22})+y'_{12}y'_{21}}{(1+y'_{11})(1+y'_{22})-y'_{12}y'_{21}}$	$s_{22} = \frac{(z'_{11}+1)(z'_{22}-1)-z'_{12}z'_{21}}{(1+z'_{11})(1+z'_{22})-z'_{12}z'_{21}}$
$y'_{ij} = y_{ij}Z_0$; $z'_{ij} = z_{ij}/Z_0$; Z_0 is the generator impedance			

	S	Y	Z
Y	$y'_{11} = \frac{(1-s_{11})(1+s_{22})+s_{12}s_{21}}{(1+s_{11})(1+s_{22})+s_{12}s_{21}}$	$y'_{11} = y'_{11}$	$y'_{11} = \frac{z'_{22}}{z'_{11}z'_{22}-z'_{12}z'_{21}}$
	$y'_{12} = \frac{-s_{12}}{(1+s_{11})(1+s_{22})+s_{12}s_{21}}$	$y'_{12} = y'_{12}$	$y'_{12} = \frac{-z'_{12}}{z'_{11}z'_{22}-z'_{12}z'_{21}}$
	$y'_{21} = \frac{-s_{21}}{(1+s_{11})(1+s_{22})+s_{12}s_{21}}$	$y'_{21} = y'_{21}$	$y'_{21} = \frac{-z'_{21}}{z'_{11}z'_{22}-z'_{12}z'_{21}}$
	$y'_{22} = \frac{(1+s_{11})(1-s_{22})+s_{12}s_{21}}{(1+s_{11})(1+s_{22})+s_{12}s_{21}}$	$y'_{22} = y'_{22}$	$y'_{22} = \frac{z'_{11}}{z'_{11}z'_{22}-z'_{12}z'_{21}}$
Z	$z'_{11} = \frac{(1+s_{11})(1-s_{22})-s_{12}s_{21}}{(1-s_{11})(1-s_{22})-s_{12}s_{21}}$	$z'_{11} = \frac{y'_{22}}{y'_{11}y'_{22}-y'_{12}y'_{21}}$	$z'_{11} = z'_{11}$
	$z'_{12} = \frac{2s_{12}}{(1-s_{11})(1-s_{22})-s_{12}s_{21}}$	$z'_{12} = \frac{-y'_{12}}{y'_{11}y'_{22}-y'_{12}y'_{21}}$	$z'_{12} = z'_{12}$
	$z'_{21} = \frac{2s_{21}}{(1-s_{11})(1-s_{22})-s_{12}s_{21}}$	$z'_{21} = \frac{-y'_{21}}{y'_{11}y'_{22}-y'_{12}y'_{21}}$	$z'_{21} = z'_{21}$
	$z'_{22} = \frac{(1-s_{11})(1+s22)-s_{12}s_{21}}{(1-s_{11})(1-s_{22})-s_{12}s_{21}}$	$z'_{22} = \frac{y'_{11}}{y'_{11}y'_{22}-y'_{12}y'_{21}}$	$z'_{22} = z'_{22}$
$y'_{ij} = y_{ij}Z_0$; $z'_{ij} = z_{ij}/Z_0$; Z_0 is the generator impedance			

APPENDIX B
DETERMINATION OF EXTRINSIC-EXTRINSIC CAPACITANCES

To determine the extrinsic-extrinsic capacitances from measurement made in deep depletion, the effective capacitances $(\Im(Y_{\Pi_{ij}})/\omega)$ of MOSFETs are approximated by the following relation

$$\frac{\Im\{Y_{\Pi_{ij}}\}}{\omega} \approx C_{ee} + \frac{C_e}{1 + \tau^2\omega^2} \tag{B.1}$$

The coefficients C_{ee}, C_e and τ^2 are determined using a mean square method. If we call $c_\imath = Y_{ij}(\omega = \omega_\imath)/\omega_\imath$ and $d_\imath = 1/(1 + \tau^2\omega_\imath^2)$, the coefficients C_{ee}, C_e, and τ^2 are found to minimize the following expression

$$\sum_{\imath=1}^{N} (c_\imath - C_{ee} - C_e d_\imath)^2 \tag{B.2}$$

After differentiating this equation for each unknows, a system of 3 equations is obtained

$$\sum_{\imath=1}^{N} (c_\imath - C_{ee} - C_e d_\imath) = 0 \tag{B.3}$$

$$\sum_{\imath=1}^{N} (c_\imath - C_{ee} - C_e d_\imath)\, d_\imath = 0 \tag{B.4}$$

$$\sum_{\imath=1}^{N} (c_\imath - C_{ee} - C_e d_\imath)\, \omega_\imath^2 d_\imath^2 = 0 \tag{B.5}$$

Equation (B.3) can be easily rewritten as

$$C_{ee} = \overline{c} - C_e\overline{d} \tag{B.6}$$

where $\overline{c}$ and $\overline{d}$ are the mean values of $c_\imath$ and $d_\imath$ respectively.

After distributing the sum in Equation (B.4), we obtain

$$\sum_{\imath=1}^{N} c_\imath d_\imath - C_{ee} \sum_{\imath=1}^{N} d_\imath - C_e \sum_{\imath=1}^{N} d_\imath^2 = 0 \tag{B.7}$$

which is simplified to

$$\frac{1}{N} \sum_{\imath=1}^{N} c_\imath d_\imath - C_{ee}\overline{d} - C_e\overline{d^2} = 0 \tag{B.8}$$

Since $C_{ee} = \overline{c} - C_e\overline{d}$ Equation (B.8) becomes

$$\frac{1}{N} \sum_{\imath=1}^{N} c_\imath d_\imath - \overline{c}\,\overline{d} + C_e\overline{d}^2 - C_e\overline{d^2} = 0 \tag{B.9}$$

If we define $s_d^2 = (1/N \sum d_\imath^2) - \overline{d}^2$, C_e can be expressed by

$$C_e = \frac{\frac{1}{N}\sum_{\imath=1}^{N} c_\imath d_\imath - \overline{c}\,\overline{d}}{s_d^2} \tag{B.10}$$

After distributing the sum in Equation (B.5), we obtain

$$\frac{1}{N} \sum_{\imath=1}^{N} \omega_\imath^2 d_\imath^2 c_i - C_{ee}\frac{1}{N} \sum_{\imath=1}^{N} \omega_\imath^2 d_\imath^2 - C_e\frac{1}{N} \sum_{\imath=1}^{N} \omega_\imath d_\imath^3 = 0 \tag{B.11}$$

By combining Equation (B.11) with Equation (B.6) and Equation (B.10), and defining the covariance, $\mathrm{cov}[x,y] = (1/N \sum x_\imath y_\imath) - \overline{x}\,\overline{y}$, yields

$$\begin{aligned} \frac{1}{N} \sum_{\imath=1}^{N} \omega_\imath^2 d_\imath^2 c_i + \frac{1}{s_d^2}\mathrm{cov}[c,d]\overline{d} \left(\frac{1}{N} \sum_{\imath=1}^{N} \omega_\imath^2 d_\imath^2\right) & \\ -\overline{c}\frac{1}{N} \sum_{\imath=1}^{N} \omega_\imath^2 d_\imath^2 - \frac{1}{s_d^2}\mathrm{cov}[c,d] \left(\frac{1}{N} \sum_{\imath=1}^{N} \omega_\imath^2 d_\imath^3\right) &= 0 \end{aligned} \tag{B.12}$$

The previous equation is then simplified to

$$s_d^2\mathrm{cov}[c, c\ d] = \mathrm{cov}[c,d]\ \mathrm{cov}[d, \omega^2\ d^2] \tag{B.13}$$

Since $\omega_\iota^2 d_\iota^2 = (d_\iota - d_\iota^2)/c_\iota$

$$s_d^2 \mathrm{cov}[c, d^2] = \mathrm{cov}[c, d]\ \mathrm{cov}[d, d^2] \tag{B.14}$$

By dividing both part of this last equation by $s_c\ s_d^2\ s_{d^2}$, and defining the correlation coefficient $\mathrm{corr}[x, y] = \mathrm{cov}[x, y]/(s_x s_y)$, the final equation is obtained

$$\mathrm{cov}[c, d^2] = \mathrm{cov}[y, d]\ \mathrm{cov}[d, d^2] \tag{B.15}$$

The equation system allowing to extract extrinsic-extrinsic capacitances is then be rewritten using Equation (B.6), (B.10), and (B.15)

$$C_{ee} = \overline{y} - C_e \overline{d} \tag{B.16}$$

$$C_e = \frac{\mathrm{cov}[c, d]}{s_d^2} \tag{B.17}$$

$$\mathrm{cor}[c, d^2] = \mathrm{cor}[c, d]\mathrm{cor}[d, d^2] \tag{B.18}$$

APPENDIX C

ALTERNATIVE USES OF THE BODY CONTACTED MOSFET

Instead of connecting the body of the transistor to the gate, the body contact can be used to create original functions in a circuit using only one device.

Active switch One possibility is to use the body contacted MOSFET as an active switch. If the potential of the body of the transistor is changed, i.e. from 0.6 to −0.6 V, the transistor can be switched from ON to OFF state. Figure C.1 shows the magnitude of s_{11} and s_{21} of the 3-ports with a gate voltage $V_{gs} = 0.5V$ and $V_{ds} = 1V$ when the potential of the body is modified. More than 15 dB of difference in transmission using a simple transistor is observed. It is interesting to note that there is only a small variation of the input parameter s_{11}. The state of the switch will not influence the circuit in front of it. But, if it is necessary to compensate a reduction of the input capacitance when the transistor is turned off, a varactor could be used.

A possible solution would be the use of a small MOSFET. Connecting its source and drain to the body contact of the active transistor, and its gate the gate of the body-contacted MOSFET allows to obtain a varactor that will increase its capacitance when the active transistor will be off (Figure C.2).

Mixer The body of the transistor can be used for more than just a switch. If variable signal is introduced into the body, due to the non-linearity of the MOSFET, it will be mixed with the gate signal. A body contacted MOSFET can then be used as a single-transistor mixer. Some tests have been done using the 3-ports, injecting a small signal into the body, at 110 MHz, and into the gate at 3 GHz. Up conversion of the body signal has been observed (Figure C.3). The highest frequency that can be used for the body signal was close to 200 MHz. When higher frequency is used, the power of the up converted signal reduces itself. For frequency higher than 5 GHz, no mixing is observed. This

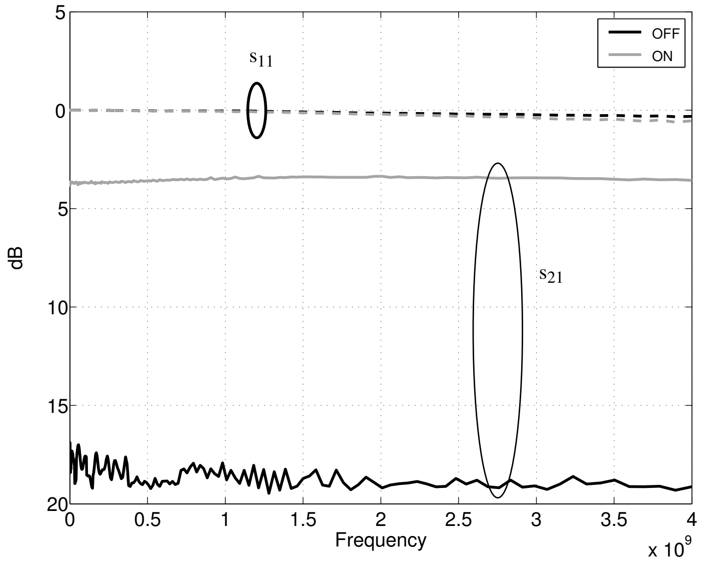

Figure C.1: Measured transmission and reflection of a body contacted MOSFET. The body potential is switched from $0.6V$ (on) to $-0.6V$ (off)

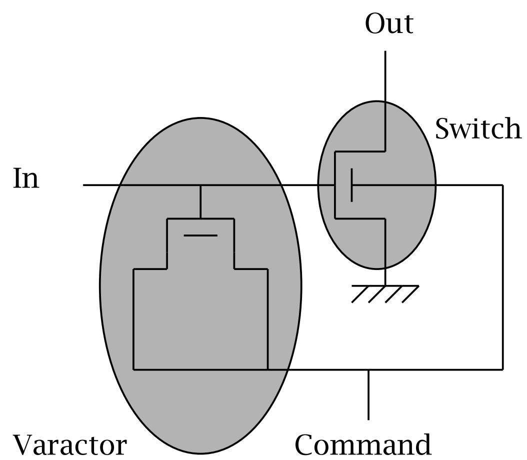

Figure C.2: Capacitive compensating circuit of the active switch.

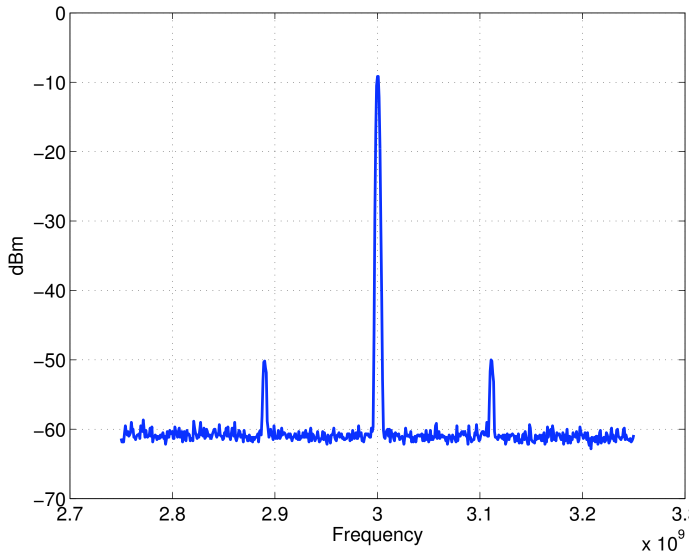

Figure C.3: Output signal, versus frequency, of a 3-ports with different signal applied at the gate (3GHz) and at the body (110MHz)

measurement confirms the limitation of the body transistor of this device, as explained in section 4.3.4.1.

APPENDIX D

MODELING OF MICROSTRIP LINES BY USING VARIATIONAL PRINCIPLE

D.1 Introduction

Variational principles are used frequently, since many years, in physics, mechanics and electromagnetics [1][2]. They are used to determine unknowns which can be expressed as a ratio of integrals involving the product of other quantities. A classical expression of a variational principle is:

$$p = \frac{\int L_1 \left[\overline{F}_i(x_1, x_2, ..., x_n) \overline{F}_j(x_1, x_2, ..., x_n) \right] dx_1 dx_2 \cdots dx_n}{\int L_2 \left[\overline{F}_i(x_1, x_2, ..., x_n) \overline{F}_j(x_1, x_2, ..., x_n) \right] dx_1 dx_2 \cdots dx_n} \qquad \text{(D.1)}$$

where $x_1 \cdots x_n$ are variables describing the domain of the problem, $\overline{F}_i$ and $\overline{F}_j$ are scalar or vector quantities associated to the problem, and L_1, L_2 denote linear combination of the product $\overline{F}_i \overline{F}_j$.

The equation (D.1) being a variational principle for the scalar p means that if the expressions $\overline{F}$ are not the exact expressions of the problem, but are satisfying some conditions related to the problem, the calculated p will not be affected significantly.

D.2 Using a variational principle

The variational principle used in this work has been proposed by Huynen *et al.* [3]. It allows to compute the propagation coefficients of a waveguide, and the power which came trough the transversal plane of this wave guide.

The waveguide can be composed of different layers with their own electrical and magnetic properties. The general expression of this variational principle is:

$$
\begin{aligned}
&\gamma^2 \int_S (\overline{a}_z \times \overline{e}^*) \cdot \left[\left(\overline{\overline{\mu}}^{-1} \cdot (\overline{a}_z \times \overline{e})\right)\right] dS \\
&+\gamma \int_S \{(\nabla \times \overline{e}^*) \cdot \left[\left(\overline{\overline{\mu}}^{-1} \cdot (\overline{a}_z \times \overline{e})\right)\right] - (\overline{a}_z \times \overline{e}^*) \cdot (\overline{\overline{\mu}}^{-1} \cdot \nabla \times \overline{e}) dS \\
&- \int_S (\nabla \times \overline{e}^*) \cdot (\overline{\overline{\mu}}^{-1} \cdot \nabla \times \overline{e}) dS + \omega^2 \int_S \overline{e}^* \cdot (\overline{\overline{\varepsilon}} \cdot \overline{e}) dS = 0
\end{aligned}
\tag{D.2}
$$

where $\overline{e}$ is the electric field in the cross-section. This equation is difficult to use for planar lines like microstrip or CPW because discontinous metallisations are present in the cross-section. But the derivation of this equation in the spectral domain simplifies the problem. After performing a Fourier transform along the x-axis on each component of the electric and magnetic fields

$$
\begin{aligned}
\tilde{e}_v(k_x, y) &= \int_{-\infty}^{\infty} e_v(x, y) e^{-jk_x x} dx \\
\tilde{h}_v(k_x, y) &= \int_{-\infty}^{\infty} h_v(x, y) e^{-jk_x x} dx
\end{aligned}
\tag{D.3}
$$

the equation simplifies into

$$
-\gamma^2 \sum_i \tilde{A}_i - \gamma \sum_i (\tilde{B}_i - \tilde{C}_i) + \sum_i \tilde{D}_i - \omega^2 \tilde{E}_i = 0 \tag{D.4}
$$

A complete development of equation (D.4) can be found in [4]. The coefficient of this last equation result from numerical integral of oscillating functions.

In the case of a microstrip line, the initial value of the electric and magnetic fields can be deduced from the longitudinal current density flowing on the strip [5]. In the spectral domain, the current density is expressed as follows:

$$
\tilde{j}_z(k_x) = 2\pi J_0(k_x W/2) \tag{D.5}
$$

where J_0 is the Bessel function of first kind and order 0, and W is the width of the strip.

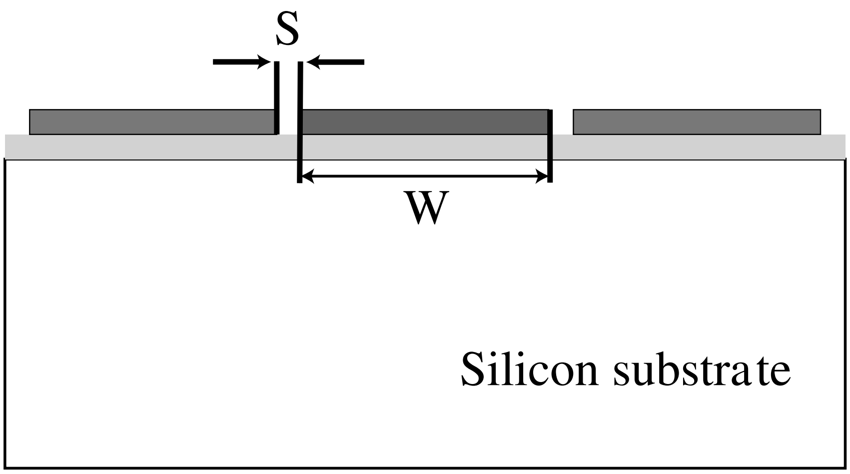

Figure D.1: Cross section of 3-coupled microstrip lines. The width of the strips and the spacing between strips are $10\mu m$ and $1\mu m$ respectively. The substrate is composed by an oxide (S_iO_2) and a silicon layer.

D.3 *Propagation modes determination of 3-coupled microstrip lines*

A device made of n-coupled lines is able to propagate n different transmission modes. A current density on the n strips is associated to each of the n modes.

Solving the problem for 3-coupled lines implies to introduce a new current density in the specral domain:

$$\begin{aligned}\tilde{j}_z &= 2\pi \Big[J_0(k_x W/2) e^{jk_x(W+S)} + \\ &\quad C_2 J_0(k_x W/2) + C_3 J_0(k_x W/2) e^{-jk_x(W+S)} \Big] \qquad \text{(D.6)}\end{aligned}$$

where W is the width of the strips, S the spacing between the strips, and C_i describes the ratio of the current flowing on the strip i and on the first strip.

In order to obtain the propagation coefficient of the 3 modes, the C_i must be determined. The analytical expressions of the propagation coefficients and the associated current distribution can be deduced from equation (5.28) for the structure presented in figure (D.1) as follows:

$$\begin{pmatrix} C_{1,1} & C_{1,2} & C_{1,3} \\ C_{2,1} & C_{2,2} & C_{2,1} \\ C_{1,3} & C_{1,2} & C_{1,1} \end{pmatrix} \begin{pmatrix} I_1 \\ I_2 \\ I_3 \end{pmatrix} = -\beta^2 \begin{pmatrix} I_1 \\ I_2 \\ I_3 \end{pmatrix} \quad (5.28)$$

The characteristic polynomial of the matrix is

$$\begin{aligned} (\beta^2 + C_{1,1} - C_{1,3}) \quad & [\beta^4 + (C_{1,1} + C_{2,2} + C_{1,3})\beta^2 \\ & -2C_{2,1}C_{1,2} + C_{2,2}C_{1,1} + C_{1,3}C_{2,2}] \end{aligned} \tag{D.7}$$

Finding the roots of this polynomial yields the expressions of the β:

$$\begin{aligned} \beta_1^2 &= -\frac{C_{1,1} + C_{2,2} + C_{1,3} + \sqrt{\varrho}}{2} \\ \beta_2^2 &= -\frac{C_{1,1} + C_{2,2} + C_{1,3} - \sqrt{\varrho}}{2} \\ \beta_3^2 &= C_{1,3} - C_{1,1} \end{aligned} \tag{D.8}$$

where $\varrho = (C_{1,1} - C_{2,2})^2 + C_{1,3}(C_{1,3} - 2C_{2,2} + 2C_{1,1}) + 8C_{2,1}C_{1,2}$

Introducing this result into equation (5.28) gives the expression of the current vectors:

$$\mathcal{I}_1 = \begin{pmatrix} 1 \\ C_2' \\ 1 \end{pmatrix} \tag{D.9}$$

$$\mathcal{I}_2 = \begin{pmatrix} 1 \\ C_2'' \\ 1 \end{pmatrix} \tag{D.10}$$

$$\mathcal{I}_3 = \begin{pmatrix} 1 \\ 0 \\ -1 \end{pmatrix} \tag{D.11}$$

where $C_2' = -\frac{(\beta_1^2 + C_{1,1} + C_{1,3})}{C_{2,1}}$, and $C_2'' = -\frac{(\beta_2^2 + C_{1,1} + C_{1,3})}{C_{2,1}}$.

The coefficient C_2', and C_2'' are determined using the Rayleigh-Ritz procedure.

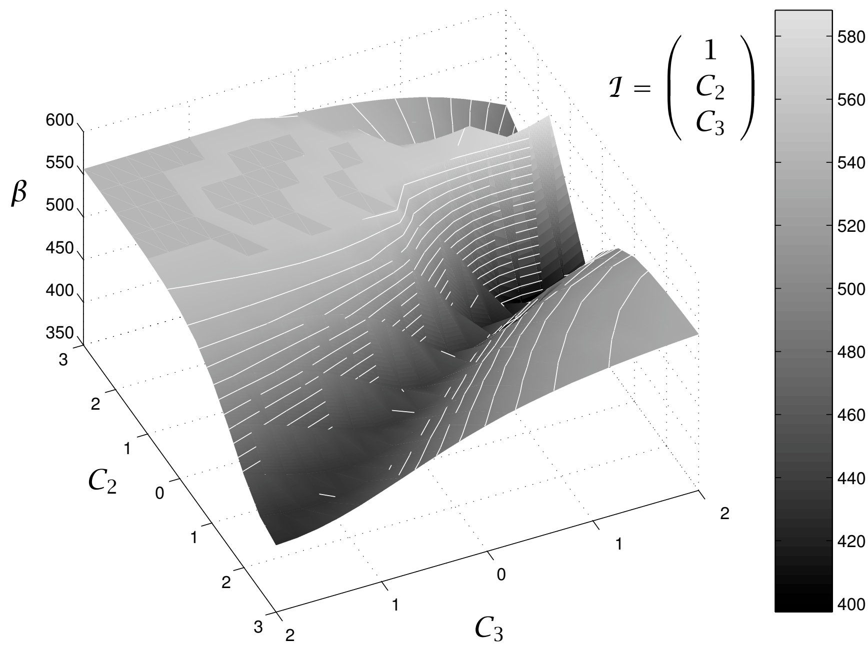

Figure D.2: Propagation coefficient of 3-coupled lines for different values of the ratio between the current flowing on the strips at 10 Ghz. The width of the lines and the spacing between the lines are $10\mu m$ and $1\mu m$ respectively. The underlaying substrate is composed of 2 layers, a 5 μm thick oxide layer (S_iO_2) and a 500 μm thick silicon layer ($\approx 20\Omega cm$).

This procedure consists of calculating the propagation constant for different C_i. The C_i solution will be the one which will produce an extremum of the curve β versus C_i. Figure (D.2) shows the surface of the β in the case of 3-coupled lines. Once the C_i are determined, the propagation coefficients and the Poynting vectors are known for each mode.

References

[1] P.M.Morse and F.Feshback, *Methods of theoritical physics*, McGraw-Hill, 1953.

[2] A. Vander Vorst and I. Huynen, *Variational Principles and Distributed Circuits*, Research Studies Press LTD Hertfordshire, England, 2000.

[3] I.Huynen, "A new variational formulation, applicable to shielded and open multilayered transmission lines with gyrotropic non-hermitian lossy media and lossless conductors," *IEEE Trans. on Microwave theory and techniques*, vol. 42, no. 11, pp. 2107–2111, Nov. 1994.

[4] I.Huynen, *Modelling planar circuits at centimeter and millimeter wavelength by using a new variational principle*, Ph.D. thesis, Université catholique de Louvain, 1994.

[5] Delinger, "A frequency dependent solution for microstrip transmission lines," *IEEE trans. on Microwave theory and technique*, vol. 19, no. 1, pp. 30–39, Jan. 1971.